Swansea University
Prifysgol Abertawe

Cronfa
Setting Research Free

Cronfa - Swansea University Open Access Repository

This is an author produced version of a paper published in :
Geomorphology

Cronfa URL for this paper:
http://cronfa.swan.ac.uk/Record/cronfa24058

Paper:
Payo, A., Hall, J., French, J., Sutherland, J., van Maanen, B., Nicholls, R. & Reeve, D. (2016). Causal Loop Analysis of coastal geomorphological systems. *Geomorphology*

http://dx.doi.org/10.1016/j.geomorph.2015.07.048

This article is brought to you by Swansea University. Any person downloading material is agreeing to abide by the terms of the repository licence. Authors are personally responsible for adhering to publisher restrictions or conditions. When uploading content they are required to comply with their publisher agreement and the SHERPA RoMEO database to judge whether or not it is copyright safe to add this version of the paper to this repository.
http://www.swansea.ac.uk/iss/researchsupport/cronfa-support/

Geomorphology 256 (2016) 36–48

Contents lists available at ScienceDirect

Geomorphology

journal homepage: www.elsevier.com/locate/geomorph

Causal Loop Analysis of coastal geomorphological systems

Andres Payo [a,*], Jim W. Hall [a], Jon French [b], James Sutherland [c], Barend van Maanen [d], Robert J. Nicholls [d], Dominic E. Reeve [e]

[a] Oxford University Centre for the Environment, South Parks Road, Oxford OX1 3QY, UK
[b] UCL Department of Geography, Coastal and Estuarine Research Unit, University College London, Gower St., London WC1E 6BT, UK
[c] HR Wallingford, Howbery Park, Wallingford, Oxfordshire OX10 8BA, UK
[d] University of Southampton, Faculty of Engineering and the Environment, Southampton SO17 1BJ, UK
[e] Swansea University, College of Engineering, Singleton Park, SA2 8PP, UK

ARTICLE INFO

Article history:
Received 1 July 2014
Received in revised form 27 July 2015
Accepted 31 July 2015
Available online 11 August 2015

Keywords:
Systems analysis
Behavioural model
Emergent behaviour
Feedback analysis
Causal loop diagram
Directed graph
High Angle Wave Instability

ABSTRACT

As geomorphologists embrace ever more sophisticated theoretical frameworks that shift from simple notions of evolution towards single steady equilibria to recognise the possibility of multiple response pathways and outcomes, morphodynamic modellers are facing the problem of how to keep track of an ever-greater number of system feedbacks. Within coastal geomorphology, capturing these feedbacks is critically important, especially as the focus of activity shifts from reductionist models founded on sediment transport fundamentals to more synthesist ones intended to resolve emergent behaviours at decadal to centennial scales. This paper addresses the challenge of mapping the feedback structure of processes controlling geomorphic system behaviour with reference to illustrative applications of Causal Loop Analysis at two study cases: (1) the erosion–accretion behaviour of graded (mixed) sediment beds, and (2) the local alongshore sediment fluxes of sand-rich shorelines. These case study examples are chosen on account of their central role in the quantitative modelling of geomorphological futures and as they illustrate different types of causation. Causal loop diagrams, a form of directed graph, are used to distil the feedback structure to reveal, in advance of more quantitative modelling, multi-response pathways and multiple outcomes. In the case of graded sediment bed, up to three different outcomes (no response, and two disequilibrium states) can be derived from a simple qualitative stability analysis. For the sand-rich local shoreline behaviour case, two fundamentally different responses of the shoreline (diffusive and anti-diffusive), triggered by small changes of the shoreline cross-shore position, can be inferred purely through analysis of the causal pathways. Explicit depiction of feedback-structure diagrams is beneficial when developing numerical models to explore coastal morphological futures. By explicitly mapping the feedbacks included and neglected within a model, the modeller can readily assess if critical feedback loops are included.

© 2015 The Authors. Published by Elsevier B.V. This is an open access article under the CC BY license (http://creativecommons.org/licenses/by/4.0/).

1. Introduction

Feedbacks and emergent behaviours in geomorphology have been long recognised (Schumm and Lichty, 1965; Schumm, 1991) but it has been in recent decades when views of change, disturbance, response and recovery have expanded considerably (Phillips, 2009): conceptual frameworks emphasizing single-path, single-outcome trajectories of change have been supplemented – not replaced – by multi-path, multi-outcome perspectives. In this context, Phillips (2009) argues that any attempt to explore change and response studies should seek to identify potential feedbacks, determine their signs, and assess their relative importance. This is especially important when studying coastal systems in which a broad range of feedback mechanisms drives the system's evolution. A feedback is a change to a component of the system that causes a knock-on effect that further alters the original change. A positive feedback amplifies the initial change. For example as waves erode the cliff, granular material will be released, which may abraid the shore platform, resulting in even more cliff erosion. Negative feedbacks have the opposite effect of the initial change. For example, as the shore platform is eroding it becomes wider and gentler diminishing the rate of mass wasting for the same given offshore wave energy flux. Identifying these feedbacks is the first step towards establishing their relevance at the spatial scales of geomorphological models (Lane, 2013). As an ever-greater number of feedbacks are identified and appreciated, the need to map them into a coherent framework is needed. Techniques for the formal assessment of the main feedbacks between coastal geomorphology and the drivers of change (i.e. climatic variability and human interventions) assist geomorphological modellers to

* Corresponding author.
E-mail addresses: andres.payo@ouce.ox.ac.uk (A. Payo), jim.hall@eci.ox.ac.uk (J.W. Hall), j.french@ucl.ac.uk (J. French), j.sutherland@hrwallingford.com (J. Sutherland), b.van-maanen@soton.ac.uk (B. van Maanen), r.j.nicholls@soton.ac.uk (R.J. Nicholls), d.e.reeve@swansea.ac.uk (D.E. Reeve).

http://dx.doi.org/10.1016/j.geomorph.2015.07.048
0169-555X/© 2015 The Authors. Published by Elsevier B.V. This is an open access article under the CC BY license (http://creativecommons.org/licenses/by/4.0/).

explore how that variability might change during the 21st century and what this might mean for geomorphic processes, landforms and entire landscapes.

The concept of feedbacks has proved helpful in the idealized model domain, but extrapolation to the real world is complicated (i.e. Klocke et al., 2013). In geomorphology examples of qualitative stability assessment of the system based on the feedback loop structure go back to at least the early 1980s (Slingerland, 1981; Phillips, 2006). The stability of the system (or conditions under which it is stable) can be determined if historical reconstructions or field observations identify the key system components and the positive, negligible, or negative links between them. This often takes the form of a directed graph, network model, or box-and-arrow diagram (Capobianco et al., 1999; Townend, 2003) (Fig. 1). These can be translated into an interaction matrix, and the stability may be determined based only on a qualitative (+, −, 0) assessment. Payo et al. (2014) have taken this qualitative analysis forward by showing how the strength (i.e. not only the sign) of a single feedback loop (e.g. the cliff toe energy depletion feedback loop) can be assessed by reasoning on the current understanding of its causal pathway. Payo et al. (2014) used directed graphs (i.e. Lane, 2000) but limited their analysis to the main processes that control the morphodynamics of cliff and shore platforms.

In this work, we extend the use of directed graphs to two different case studies: (1) processes that control the erosion–deposition behaviour of graded beds, and (2) processes that control the local alongshore sediment transport fluxes of sand-rich shorelines. These case studies are selected because they are illustrative of how directed graphs can be used to capture different types of causation, and because of their central role in the quantitative modelling of geomorphological futures. When modelling geomorphological futures at decadal and longer timescales, the modeller is likely to make informed decisions about how to numerically model the fundamentally different behaviour of mixed sediments versus uniformly graded ones. Le Hir et al. (2011) noted the need for any morphodynamic model of mixed sediment to add an active layer concept to deal with the erosion of the different fractions. Explanations of shoreline behaviours not captured by a purely diffusive 1-line approach (Ashton et al., 2001; Van den Berg et al., 2011), and attempts to unify the quantitative modelling of a graded beach has been published elsewhere (van Rijn et al., 2007). However, to the authors' knowledge, no attempt to synthesize the feedback structure of these case studies in a unified way has yet been presented.

This manuscript is organised in four main sections. In Section 2, we present the rationale for this study and define the symbolic convention adopted in this work. The feedback structures for each of the study cases are presented in Sections 3 and 4. To conclude, we highlight the benefits and limitations of our advocated qualitative modelling approach.

2. Methodology

Of the varied representational approaches within the field of systems dynamics two predominate: Causal Loop Diagrams (CLDs) and Stock and Flow Diagrams (Lane, 2000). CLDs are a broad representations of the variables and feedback structure while, in contrast, Stock and Flow Diagrams are more detailed, discriminating both state and flow variables. These two forms are fairly standardised and while their benefits and limitations are generally understood (Morecroft, 1982), the preference for one over the other is still contested (Lane, 2000); both conventions have been used in the past for conceptualizing decadal to centennial coastal system dynamics (Fig. 1). For example, Townend (2003) used stock/flow system diagrams to represent coast and estuarine system behaviour and Capobianco et al. (1999) proposed the use of CLDs to assess the impact of sea-level rise on estuaries and adjacent coasts. From a model development perspective, it might be argued that stock and flow diagrams provide more information to guide the organisation and structure of model code developed from them. Here, however, we are interested in the identification of the feedback loop structure, and the use of directed graphs is favoured. While the most relevant literature at which the conceptualization presented here is built upon is cited, the authors acknowledge that is not possible to cite the entire significant body of literature.

Fig. 2 shows the symbolic convention used in this work. The hierarchy of levels is captured by a cluster of variables at each level (c.f. Phillips, 2012). The terms 'local' and 'global' are used in the broadest sense to refer to scale finer, shorter and more detailed, or coarser, longer and broader, respectively, than the scale of observation. The term 'scale' is also used in a broad sense, encompassing both spatial and temporal resolution and position within a hierarchy. For the sake of clarity, a minimal set of symbols is used to capture causality and feedback loop structure. This includes:

- Two types of variables: (1) state variables (stocks, levels, attributes) (e.g., beach width, dune volume, sea level, sediment size, threshold wind velocity for initiating sediment transport), and (2) rate variables (underlined) (flows) (e.g. rate of shoreline change, sediment transport rate).
- Positive (+), negative (−) or influence (+/−) links. Links connect two variables (e.g. X → Y) and represent the answer to the question if X increases, would Y increase or decrease compared to what it would otherwise have been? Links are positive if $dy/dx > 0$ or negative if $dy/dx < 0$. When the answer is not known or ambiguous it is represented as an influence link.
- Causal pathways. We can reason about the influence of one variable on another variable indirectly connected to it by examining the

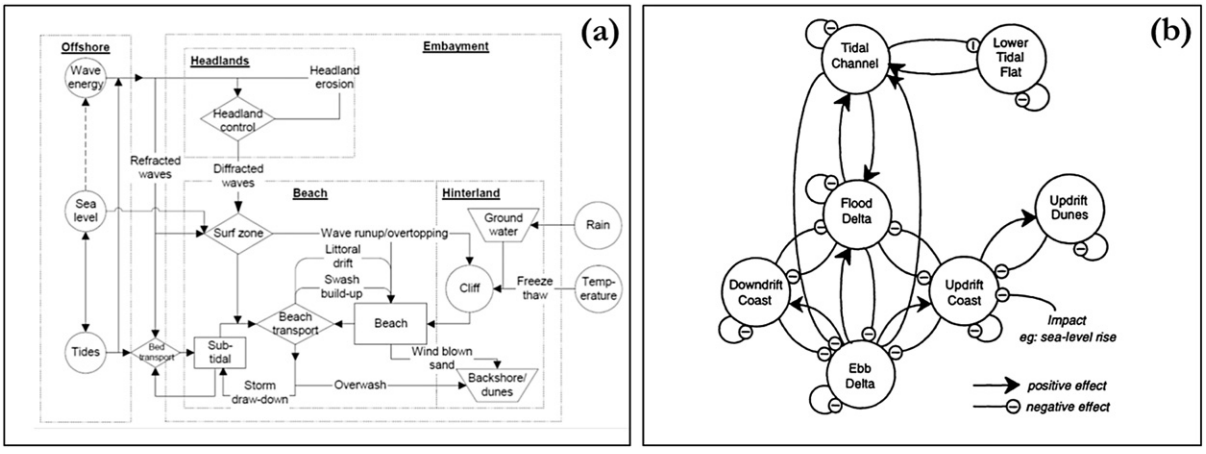

Fig. 1. Examples of how stock and flow and causal loop diagrams have been used to represent coastal system functioning and behaviour for different purposes. (a) Stock and flow diagram of an embayment (Townend, 2003) and (b) causal loop diagram of the impact of sea-level rise on an inlet or lagoon entrance (Capobianco et al., 1999).

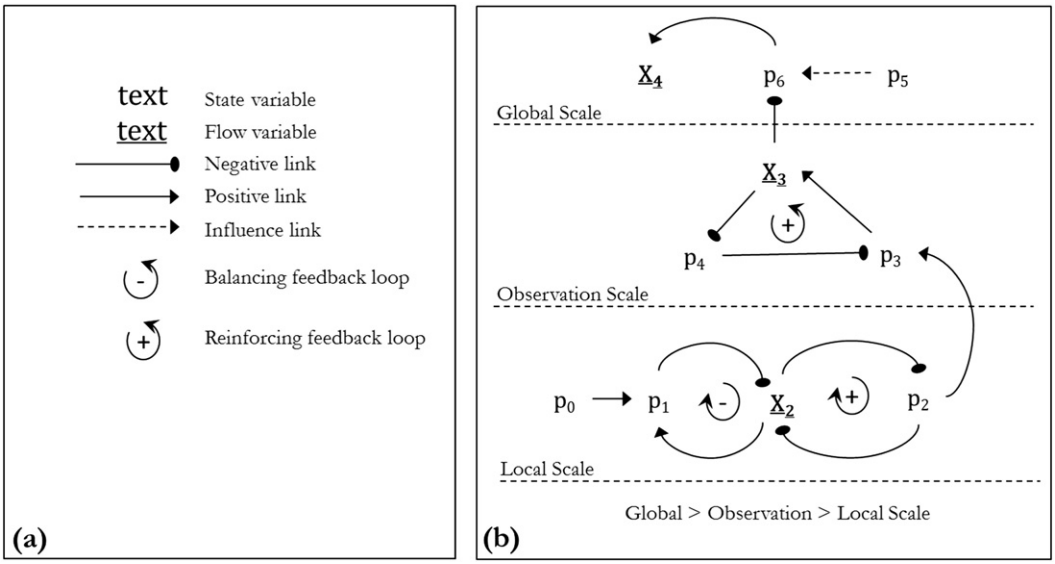

Fig. 2. Convention used to represent the causal loop diagrams in this paper. (a) Symbolic convention and (b) example application of scale hierarchy at three scales (Global > Observation > Local). The directionality of the link is represented by the arrow and oval head for the positive and negative link respectively.

signs along their causal pathway (e.g., two negatives, whether adjacent or not, will act to reverse each other). Loops in a causal loop diagram indicate feedback in the system being represented. In this case, changes cascade through other factors so as to either amplify (reinforcing feedback; products of signs positive) or dampen the original change (balancing feedback; products of signs negative).

3. Mapping graded sediment erosion–accretion behaviour

Building on field and laboratory observations of the active layer (Fig. 3), a conceptualization of the bottom elevation in terms of disequilibrium between erosion and accretion processes (Fig. 4), and the behaviour of a graded (i.e. mixed non-cohesive and cohesive) sediment bed (Fig. 5) can lead to a CLD that synthesizes how a generic active layer behaves (Fig. 6). Bottom elevation is defined as the elevation difference between the seabed/beach surface and a datum defined well below the active layer.

3.1. Feedback structure

The active layer (Fig. 3a) represents the thickness (O(10 cm)) of the surficial sediment that is affected by hydrodynamic processes (essentially waves and currents) over timescales of a few minutes (mixing depth) or hours to the tidal cycle or several days (disturbance depth) (Harris and Wiberg, 1997). From field observations, Anfuso (2005) found that the thickness of the active layer averaged over the surf-zone correlates linearly with the surf scaling parameter (Guza and Inman, 1975), being greater for reflective sand beaches (20%–40% of the significant wave height at breaking H_s) and lower for more dissipative sand beaches (i.e. 1%–4% of H_s) (Fig. 3b). Yamada et al. (2013), based on a series of laboratory experiments, have observed how the active layer is not spatially homogeneous but varies across-shore for regular spilling breaker and intermediate beach states. The sediment content of the active layer is represented by the volumetric content of different fraction sizes [$\Phi_{total} = f(\Phi\boldsymbol{coarse}, \Phi\boldsymbol{sand}, \Phi\boldsymbol{mud}, \Phi\boldsymbol{water})$]. By definition of the state variable total sediment volumetric content, a decrease (or increase) in bed volume sediment content decreases (or increases) the averaged bottom elevation relative to a datum defined well below the active layer ($d(Av.\ bottom\ elevation)/d\Phi_{total} > 0$). A change in average bottom elevation has a negative effect on average water depth over the active layer ($d(Ave.\ water\ depth)/d(Av.\ bottom\ elevation) < 0$) (Fig. 3c).

The disequilibrium condition between sediment concentrations and shear stress (especially for finer sediment fractions) has been analysed by treating sediment entrainment and deposition independently (Houser and Barrett, 2010). Bed elevation change (dz/dt) can be estimated through the conservation of sediment as the difference between the instantaneous sediment entrainment and deposition (Nielsen, 1992) or as a balance of time-averaged upward suspension potential and the amount of sediment settling from the water column (Kobayashi and Johnson, 2001) (see Fig. 4a). Independently of the parameterization used, bed elevation change at the active layer scale can be represented as a balance of volumetric erosion and deposition rates (Fig. 4b). Both deposition and erosion rates are balanced by the depletion of depth-averaged suspended sediment and depletion of erodible sediment respectively; both can thus be depicted as balanced feedback loops. The settling velocity of the mixed fraction is influenced by the finer sediment fraction through flocculation and hindered settling (van Rijn, 2007). Flocculation increases the effective diameter and settling velocity, while hindered settling reduces the settling velocity due to flow and wake formation around the particles and an increase in the density and viscosity of the suspension. Flocculation is a dynamically active process that readily reacts to changes in hydrodynamically-generated turbulent shear stresses (τ) and Suspended Particulate Matter (SPM) concentration (Eisma, 1991; Benson and French, 2007), together with salinity, mineralogy and biological stickiness (Manning et al., 2013). While the importance of bio-chemical processing processes on the suspended sediment behaviour has been long recognised, there is presently no agreement on the sign of their net effect on settling velocity; this is therefore represented as an influence link in Fig. 4c.

The erosional behaviour of graded sediments has been synthesized by van Ledden et al. (2004), and the extensive laboratory and field data have been reviewed separately by van Rijn et al. (2007), and modelling approaches reviewed by Le Hir et al. (2011). Laboratory and field observations suggest that the erosion rate is proportional to the difference between the critical bed shear stress for erosion (τ_{crit}) and the actual bed shear stress (τ) to a power, ns, with ns being higher for smaller particles, inducing the bed armouring or increase in D_{50} (i.e. loss of finer fractions of active bed layer; Le Hir et al. (2011); Fig. 5a). The energy dissipation due to wave breaking and bottom friction (i.e. wave and current) has been found to be a robust proxy for near-bed shear stress due to wave breaking and bottom friction (Kobayashi

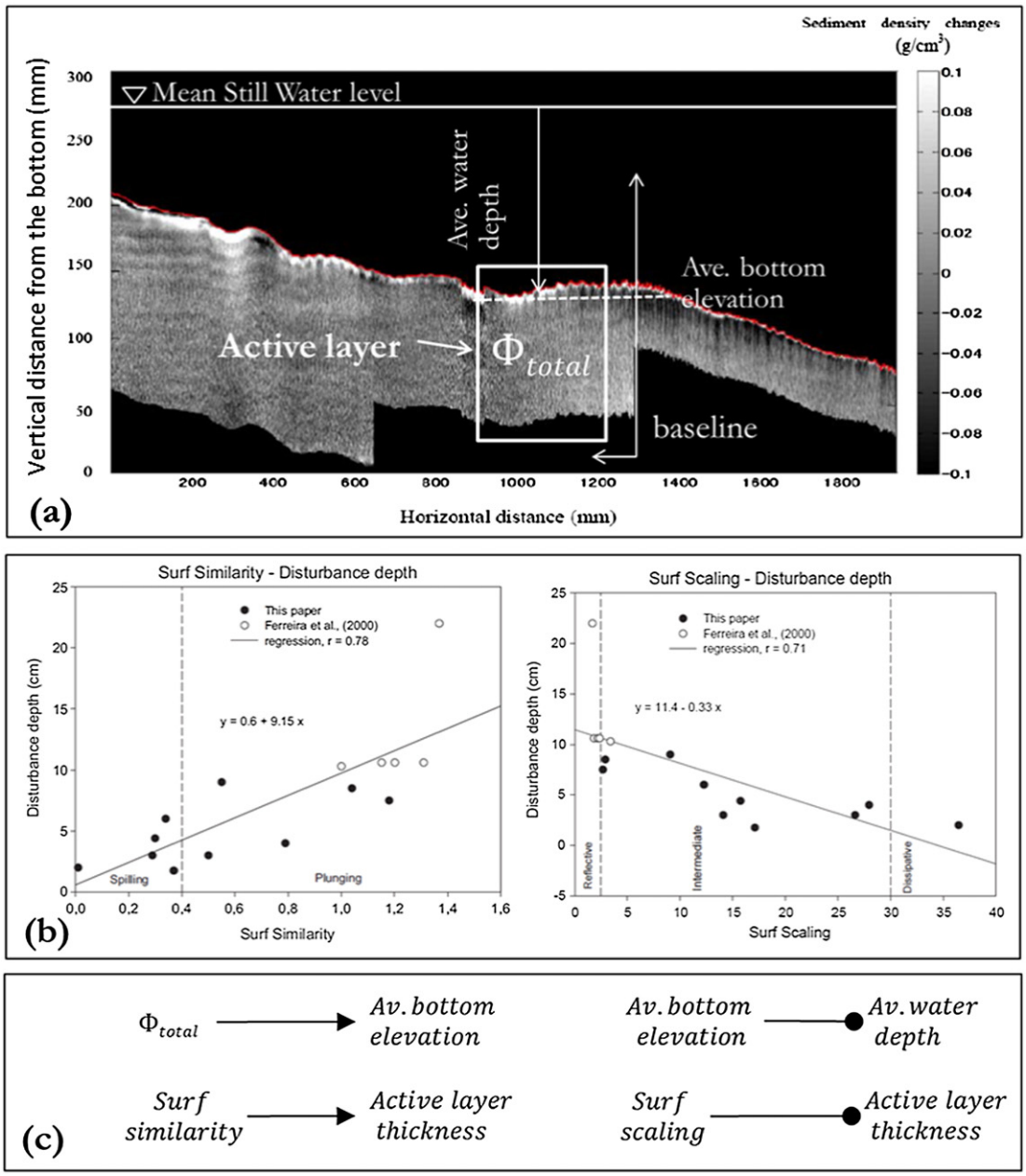

Fig. 3. (a) Active layer represented as a white rectangle over an observed across-shore variation of a sand bed in a flume subject to regular wave forcing. Red line indicates the sediment surface after 5.5 h of wave forcing. Sediment density is represented relative to the initial density on a grey scale. Lighter (darker) colours indicate a decrease (increase) in density (modified from Yamada et al. (2013) published with permission of Journal of Coastal Research). (b) Field observation of the averaged active layer thickness over the entire surf-zone shows positive (negative) correlation with the surf similarity (surf scaling) parameter (from Anfuso, 2005). (c) Above relationships represented using CLD symbolic convention.

et al., 2008; Houser and Barrett, 2010). Ripple height and steepness are well known to increase the energy dissipation due to bottom friction but ripples are also influenced by the energy dissipation itself (Nielsen, 1992). Given that this synthesis focuses on the active layer scale, at which ripples are averaged into a time and space averaged bottom elevation, their self-organising behaviour and dependence on energy dissipation (represented as influences in Fig. 5b) are not explored further (see also the work of Coco et al. (2007a) for examples of the complexities of ripple behaviour). Bio-geochemical processes have been found to either increase or decrease the critical shear stress (Friedrichs and Perry, 2001a; Friedrichs, 2011) and are also represented as an influence link. For a uniform bed, the critical shear stress increases with the sediment size (e.g. D_{50}). For a non-uniform bed, the armouring of an eroding bed further influences bed erosion by: (1) increasing the critical shear stress of the finer particles and decreasing the critical shear stress of the coarser particles due to a hiding effect (ξ) and (2) increasing effective bed shear stress of the coarser fraction and decreasing that of the finer (skin friction modulation, λ) (Fig. 5b, c) (van Rijn, 2007). In particular, van Rijn (2007) found that $\xi \approx (D_i/D_{50})^{-1}$ and $\lambda \approx (D_i/D_{50})^{-0.25}$ for mixed sands. The critical shear stress to initiate sediment transport also depends on other factors that determine the vertical strength profile of the bed. van Ledden et al. (2004) proposed the use of the liquidity index and the degree of packing to explain the erosional behaviour of unconsolidated sediment mixtures (Fig. 5c). They reported a more gradual transition from non-cohesive to cohesive behaviour when the network structure becomes silt-dominated, and a sharp transition when the structure is sand-dominated. Critical shear stress increases with sediment size of mixed sediments when the mud fraction ranges

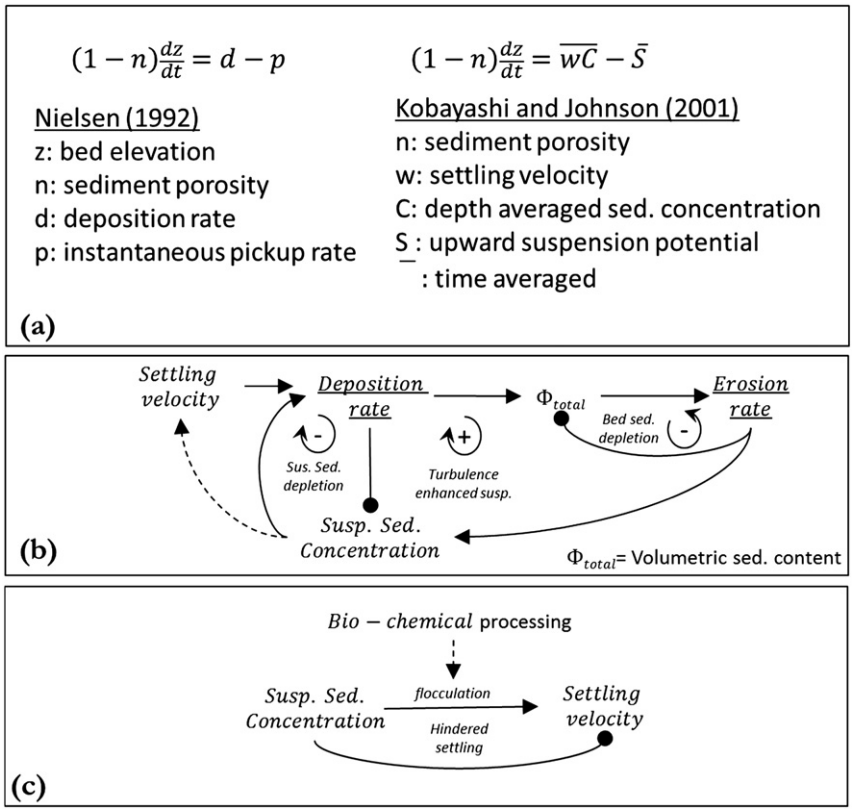

Fig. 4. At the active layer scale, bed elevation can be understood as a balance between deposition and entrainment. (a) Examples of instantaneous and time-averaged parameterizations of deposition and entrainment rate. (b) Bed elevation change represented in CLD form including the supply feedbacks of suspended sediment and bed sediment. Eroded sediment from bed, at this scale, is transferred to the suspended sediment concentration. (c) For the mud fraction; flocculation and hindered settling also control the settling velocity of the mixture. No agreement exists on the sign of the bio-chemical processing influence on suspended sediment concentration, partly due to the limited field observations but also due to the wide range of potential interactions and circumstances involved.

from 20%–40%, and critical shear stress is dominated by cohesive forces when the mud content exceeds about 70% (Le Hir et al., 2011).

Erosion rate and deposition rate are balanced due to water flux continuity and depletion of wave and current transport capacity associated with water depth (and therefore bed level) changes (Fig. 6a). Due to water continuity, an increase in water depth (i.e. erosion of the bed) reduces the depth-averaged current velocity. Since energy dissipation due to bottom friction is proportional to the velocity amplitude, this leads to a decrease in energy dissipation rate. An increase in water depth, for a given wave height and period, decreases the maximum wave orbital velocity at the bottom (i.e. proxy for near-bed turbulence) until the wave base is reached. Additionally, an increase in water depth reduces depth-induced breaking. Collapsing all the above-mentioned pathways translates into a negative effect between the water depth and total (current plus wave) energy dissipation rate. Fig. 6b combines the active layer links discussed in this section into a single diagram. The effect of bed compaction induced by packing has been also included as a negative link between degree of packing and bed elevation.

3.2. Upward causation

We now illustrate how the proposed feedback structure of the erosional and depositional behaviour of a graded sediment bed can be used to capture an upward causation effect by which small-scale processes influence morphological changes at much larger time and space scales. To this end, we explore the elevation changes in tidal flats and their ability to keep pace with sea-level rise. In particular, we link the dominance of different loops with three distinct anticipated behaviours.

The ability of tidal flats to keep pace with sea-level rise is not only influenced by the sediment mass balance (i.e. accretion deficit or surplus) but also the elevation deficit that incorporates the additional effect of shallow subsidence by autocompaction and shrinkage of the sediment layer (Cahoon et al., 1995; Allen, 1999; French, 2006). Compaction is largely driven by time evolution of the effective stress within the sediment column (Allen, 1999; Brain et al., 2011), but also by shrinkage due to desiccation (Van Wijnen and Bakker, 2001). These processes can be represented (Fig. 7) by two causal pathways that influence the degree of packing (compaction) and both packing and sediment strength directly (desiccation and wetting). Compaction reduces the erosion rate by reducing sediment liquidity and increasing packing. The increase in critical shear stress shifts the balance between the local (i.e. non-advected) erosion/deposition rate and bed elevation (see grey thicker causal pathway in Fig. 7b). Compaction not only increases the critical shear stress but also reduces the bed elevation relative to water level. An increase in relative water level reduces the dissipation of wave and current energy, thereby further decreasing the erosion potential. While elevation deficit might be dominant on minerogenic tidal flats, the authors acknowledge that biological activity can further contribute to both the sediment budget and the erosion potential (e.g. diatom mucilage can significantly increase the critical shear stress (Paterson, 1997)).

More generally, the existence of multiple feedback loops in Fig. 7 means that the active layer can exhibit three qualitatively different behaviours. Fig. 8 sketches these as a function of the total bed shear stress and the time-averaged water depth, as a proxy for bed erosion potential. Since the bed stress reaches a minimum when water depth tends either to zero or close to tidal high water, the bed-shear stress variation with averaged water depth (black solid line in Fig. 8) must have a maximum between these two limits. For a bed layer of mono-sized sediment (i.e. no hiding effect, armouring or fine wash-over effect), the critical shear stress for entrainment is independent of the "bed memory" (i.e. history of maximum bed shear stress) and can be represented as a constant value. Where this straight line coincides with the bed shear stress it

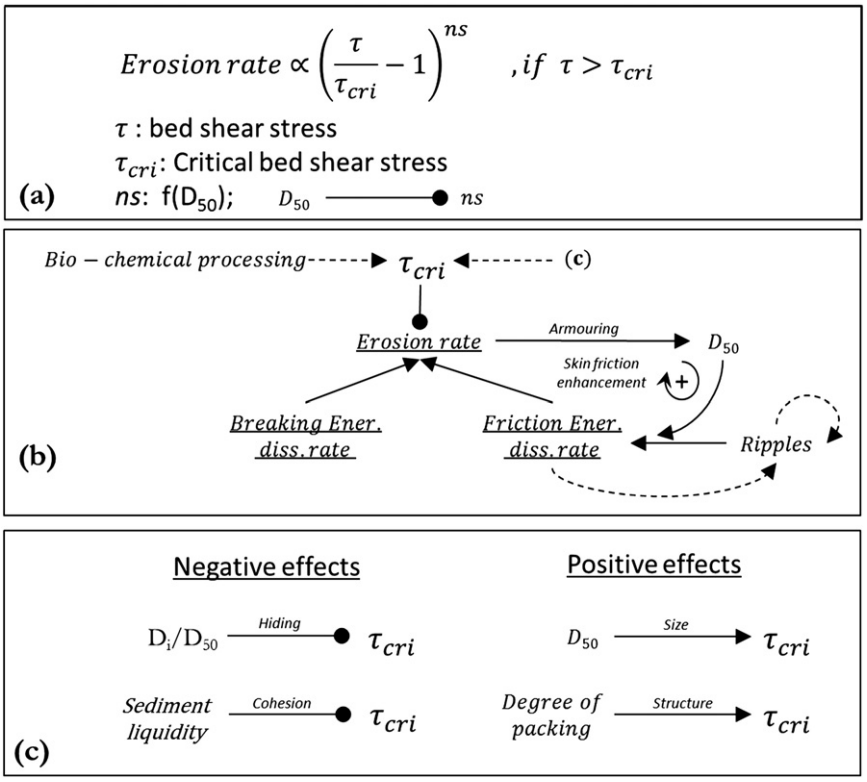

Fig. 5. The volumetric sediment erosion rate is proportional to the difference between a critical shear stress and the actual bottom shear stress. (a) This expression can be generalized as a power function where the exponent, *ns*, is higher for smaller particles. (b) Erosion rate expression represented as a CLD. Bio-chemical processes influence the threshold shear stress but no agreement on the sign has emerged. The actual bottom shear stress is function of the energy dissipation rate due to wave breaking and bottom friction (i.e. wave and current). The armouring effect of an eroding-graded-bed reinforces erosion of bed material by enhancing the skin friction. (c) A graded bed also influences erosion either by increasing or decreasing the critical shear stress for erosion.

represents an equilibrium depth where bed-shear stress is just insufficient to erode the bed. A stable solution (dark circles) also occurs when a positive (negative) perturbation of the equilibrium depth is counteracted by increased (decreased) erosion. Conversely, instability (empty circles in Fig. 8) occurs when a perturbation of the equilibrium depth causes evolution away from the stationary solution, either by further reducing the water depth (i.e. siltation) or towards a stable deeper water condition. For mixed sediments, the hiding effect, armouring and winnowing become active and the critical shear stress becomes dependent on the memory of the bed. At lower bed shear stress, the finer fractions are quickly washed out, such that a lag deposit of coarser grains armours the bed, hiding the remaining finer material from further erosion. The system might eventually achieve a stable state when armouring is the dominant effect, in which case the stable critical shear stress will depend on both the bed-shear history and the fraction of coarser material in the bed (i.e. higher shear stresses for mixed sediment with richer coarser fractions). For the example illustrated in Fig. 8, the behaviour of both mixed and single sized bed sediment, subject to the same initial critical shear stress is compared. Depending on the bed-shear stress history (shown here as a simple sigmoidal variation of bed shear–stress), the bed elevation (or equivalently averaged water depth) exhibits two equilibria — one stable and one unstable. These are closer together for the case of the non-graded bed (i.e. less resilience) than for the graded cases, and may even be disconnected from the shear stress due to elevated critical shear stresses (e.g. loss of sediment water content, or tidal inlets where the channel has reached a hard bottom).

4. Mapping sand-rich shoreline local planform behaviour

In this section, we shift our attention to the landform scale and demonstrate how our current understanding of the processes that control the beach plan-form can be synthesized into a CLD.

4.1. Feedback structure

On an open, long, sand-rich coast, wave-driven alongshore sediment transport tends to smooth the coastline if the angle between deep water wave crests and the shoreline is relatively small (Komar, 1998). However, for waves approaching at a large angle with respect to the shoreline, the gradients in alongshore drift may reinforce nearshore-bathymetry irregularities, rendering the rectilinear coast unstable (Ashton et al., 2001). This instability, termed High Angle Wave Instability (HAWI), has been used to explain persistent shoreline features over a large range of spatial scales, such as cuspate shorelines, alongshore sand waves, and flying spits (Ashton and Murray, 2006). Whereas earlier studies have pointed only to the alongshore drift as the cause of the instability, Ashton and Murray (2006) have shown that the instability mechanism involves both the surf and the shoaling zones, so that the link provided by the cross-shore sediment transport becomes crucial. Falqués et al. (2011) have shown that obliqueness of wave incidence has two effects on the alongshore drift: (i) a direct effect on the relative angle between the wave fronts and the shoreline, and (ii) an indirect effect on breaker height via the wave energy spreading during refraction. The direct effect is always stabilizing, and instability occurs only from the effects of wave energy spreading, which dominates at large incidence angles. In the following, we show how this system behaviour can be captured using CLDs.

Let us define the across-shore location of the shoreline and depth of closure at the observation point, x_{obs}, as, y_s, and y_c respectively, as shown in Fig. 9. The adjacent locations to the left and to the right of the observation point are x_l and x_r respectively, being the alongshore distance between each point to the observation point (equal to dx). The alongshore sediment transport, Q, is positive in the x direction or global alongshore coordinate, and the alongshore sediment transport gradient at the

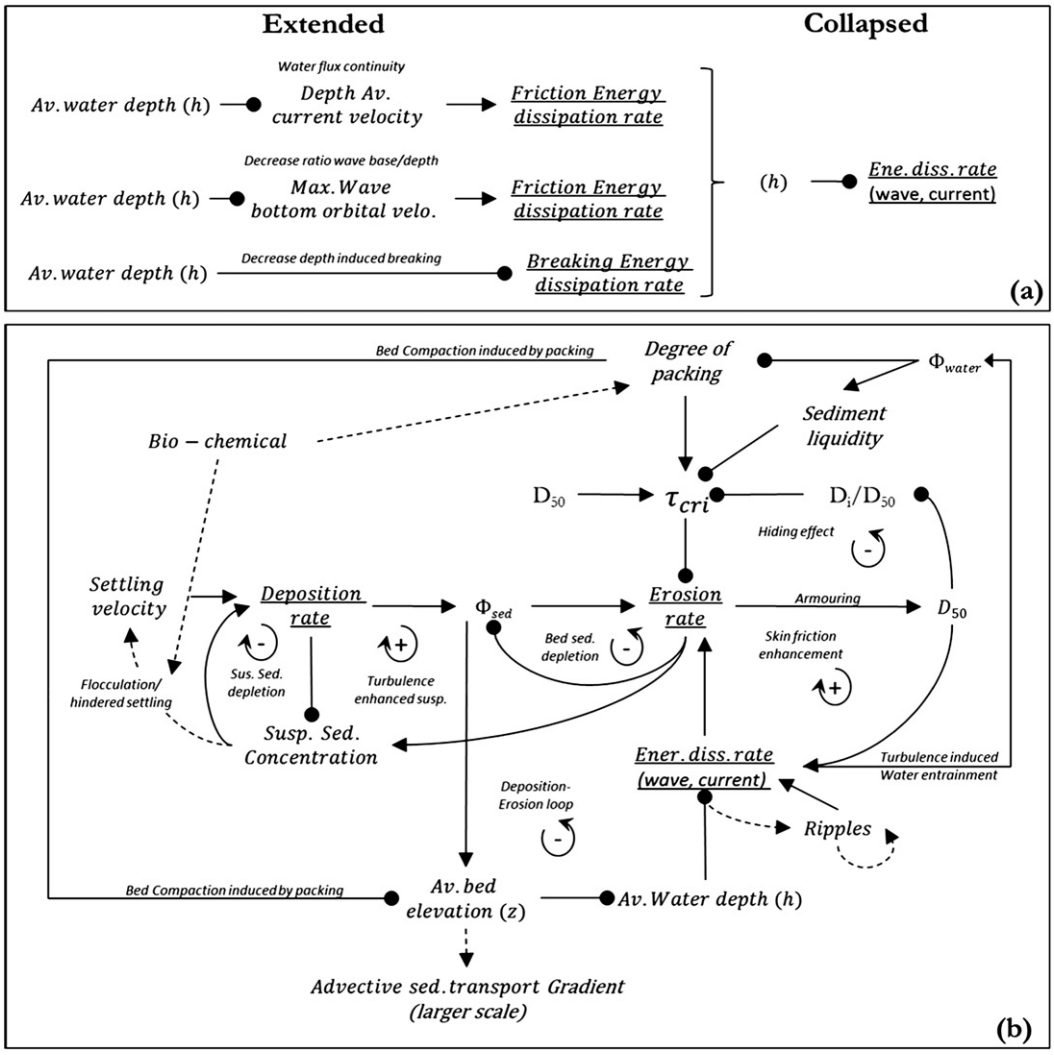

Fig. 6. Synthesis of the erosional and depositional behaviour of bottom sediment at the active layer scale. (a) Causal pathway between bed elevation change and energy dissipation due to waves and currents is collapsed into a single negative effect. (b) Overall loop structure, showing the dynamical behaviour of local eroded/deposited sediments only (i.e. advected sediment not represented here but at higher scales as sediment transport gradients).

observation location, at a given time, is defined as:

$$\frac{dQ}{dx} = \frac{Q(x_r) - Q(x_l)}{dx} \tag{1}$$

where:

$$Q(x_r) \approx H_{b,r}^{5/2} \sin\left(2\left(\theta_{b,r} - \Phi_{s,r}\right)\right) = H_{b,r}^{5/2} \sin\left(2\alpha_{b,r}\right) \tag{2}$$

and:

$$Q(x_l) \approx H_{b,l}^{5/2} \sin\left(2\left(\theta_{b,l} - \Phi_{s,l}\right)\right) = H_{b,r}^{5/2} \sin\left(2\alpha_{b,l}\right) \tag{3}$$

are the Q values at the right and left side of the observation point, $(H_{b,l}, H_{b,r})$ being the wave height at breaking, $(\theta_{b,l}, \theta_{b,r})$ wave angle at breaking and $(\Phi_{s,l}, \Phi_{s,r})$ the shoreline orientation at the left- and right-hand side of the observation point. Based on this plan-form schematization, an increase in $\frac{dQ}{dx}$ has a negative effect on the sediment volume at the observation point, and therefore on shoreline position. An advance of the shoreline position at x_{obs} increases the shoreline angle relative to the x axis at the left-hand side, $\Phi_{s,l} = \frac{y_s(x_{obs}) - y_s(x_l)}{dx}$, and decreases the shoreline orientation at the right-hand side, $\Phi_{s,r} = \frac{y_s(x_r) - y_s(x_{obs})}{dx}$. Similar reasoning applies to the orientation of the depth of closure to the left, $\Phi_{c,l} = \frac{y_c(x_{obs}) - y_c(x_l)}{dx}$ and right, $\Phi_{c,r} = \frac{y_c(x_r) - y_c(x_{obs})}{dx}$ of the observation point. Therefore, the effect of increasing y_s or y_c is always positive on the orientation of any bathymetric contour at the left-hand side and negative at the right-hand side. Next, we need to answer the question of what are the effects of a shoreline advance on the alongshore sediment transport gradient at each side of the perturbation?

For waves at breaking (typically $\propto_b \ll 45°$ because of refraction and therefore $sin2 \propto_b \approx 2 \propto_b = 2(\theta_b - \Phi_s)$) an increase of shoreline orientation, Φ_s, has always a negative effect on the alongshore sediment transport. The latter applies to changes in shoreline orientation but not to other bathymetric contours or depth of closure as explained below. A causal pathway analysis (Fig. 10a) shows that an advance in shoreline position, always has a positive effect on the alongshore sediment transport gradient. In line with conventional Causal Loop Analysis (Morecroft, 1982), this follows from the sequence of signs: $+ - + - =$ $+$ from left and $- - + + = +$ from the right. This is then collapsed into a positive link between shoreline positions and alongshore sediment transport gradient. However, the alongshore sediment transport gradient has also an indirect effect on shoreline position by changing the shoaling contours. While the alongshore sediment transport is driven by the wave angle at breaking, sediment is transported further offshore from the breaking point down to the depth of closure. This

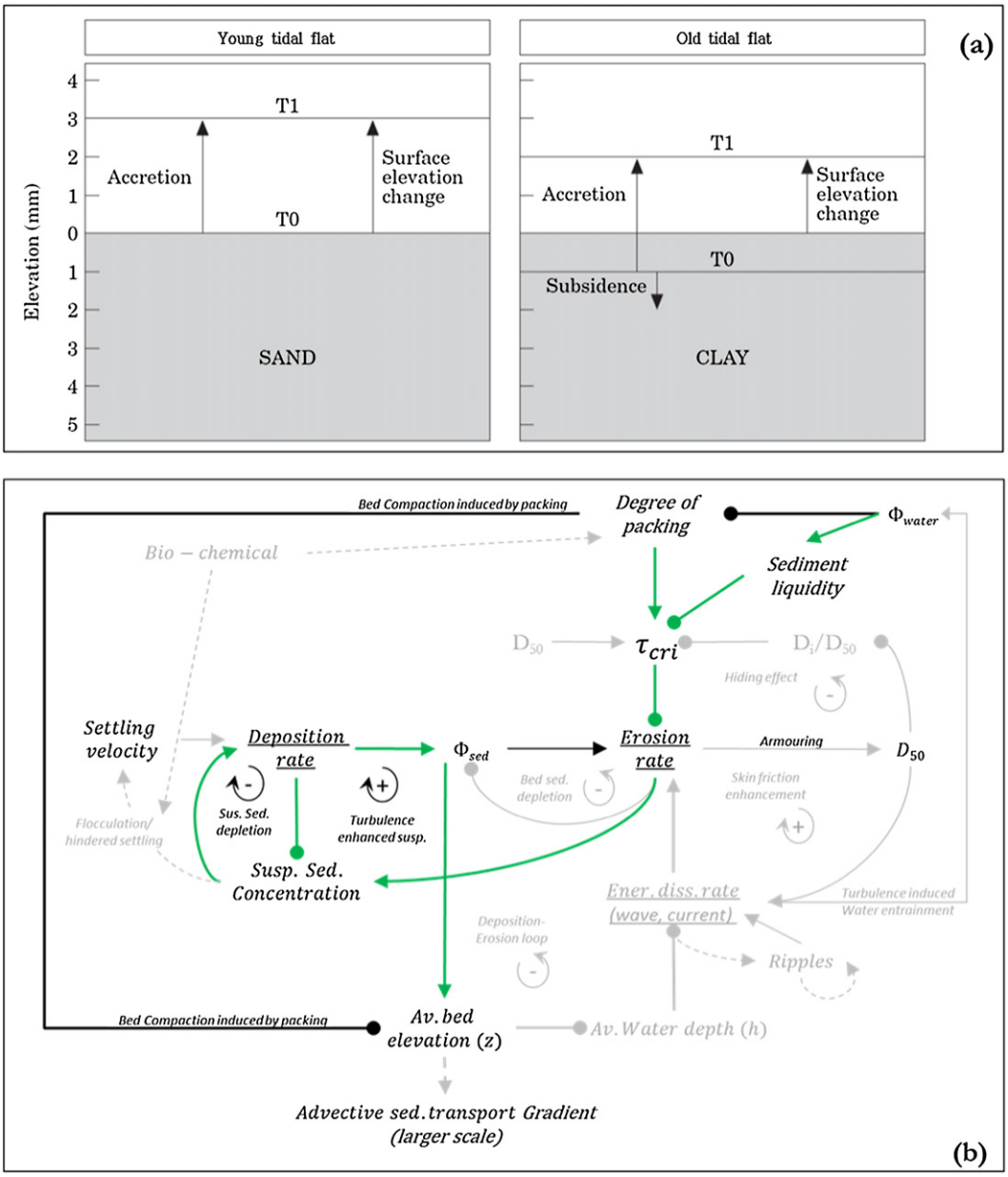

Fig. 7. An elevation deficit within a tidal flat sedimentation system can be conceptualized as a direct and non-direct large-scale consequence of a set of processes at the active layer scale; a) shows the differences in elevation at initial stage (T0) and final stage (T1) of a young (sand-reach) and old tidal flat (clay-rich) (Van Wijnen and Bakker, 2001); b) direct effect of changes on seabed sediment volumetric water content (black) and non-direct effect (green) on averaged sea bed elevation. Direct effects are likely dominant in young tidal marshes and non-direct on old tidal flats.

transport is explained by the spiral velocity profile resulting from vector addition of the alongshore and across-shore currents (Svendsen and Putrevu, 1994). Therefore, a perturbation of the shoreline propagates seaward to the shoaling zone, affecting the wave angle and height at breaking, and therefore the sediment transport gradient. As shown by Falqués et al. (2011), an increase in the offshore wave angle relative to the shoaling bathymetry contour always has a negative effect on wave height at breaking due to energy spreading. The actual magnitude of the effect will depend on the shoaling geometry (they assumed this to be parallel and rectilinear). Causal pathway analysis shows that an advance in depth of closure contour always has a negative effect on the alongshore sediment transport gradient, either from the left-hand side $(+--+-=-)$ or right-hand side $(---++=-)$ due to a reduction in wave energy because of energy spreading (Fig. 10b). Energy spreading also affects the wave angle at breaking (i.e. very oblique waves arrive at the shore with smaller height and break in shallower water causing a decrease in $\propto_b$) adding a negative effect on the alongshore sediment transport gradient (Fig. 10c). The resulting CLD for the open coast, including the existence of a local sink or source of sediment ($q(x_{obs},t)$) and the balanced feedback loop between erodible sediment volume, V_{sed}, and alongshore sediment transport gradient is shown in Fig. 10d. A reduction in V_{sed} reduces the outgoing (Q_r) sediment transport rate, relative to the potential sediment transport (Hanson and Militello, 2005), and therefore a positive effect on the alongshore sediment transport gradient. The resulting balanced feedback loop (termed "sediment depletion" in Fig. 10d) indicates that the alongshore sediment transport gradient can also be controlled by a lack of sediment and not only a reduction of transport capacity due to beach plan-form rotation (here termed "transport depletion").

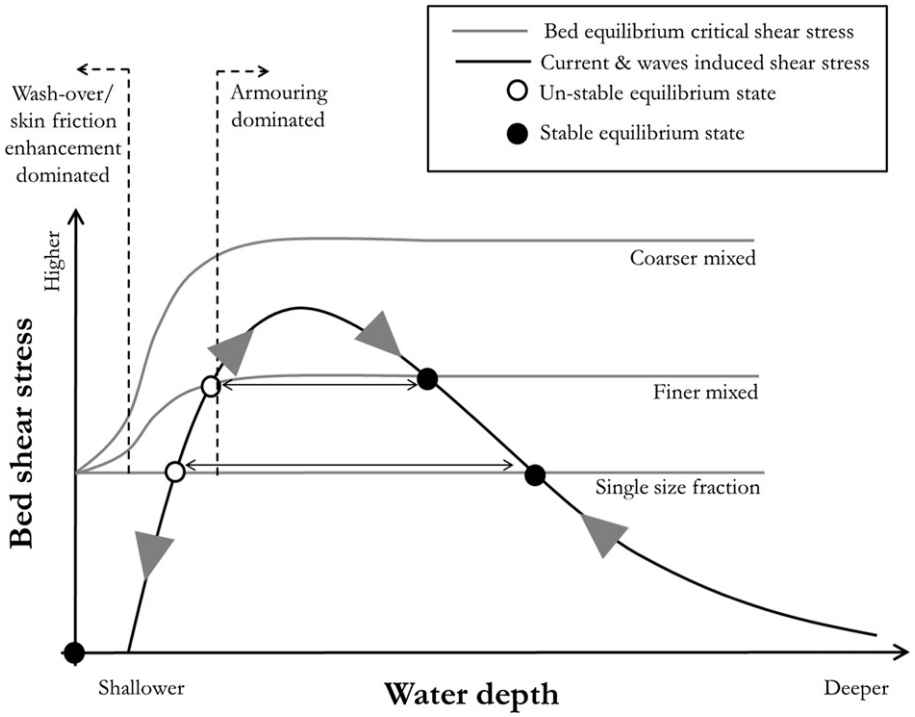

Fig. 8. Qualitative stability diagram of active layer behaviour based on the feedback structure of erosion–deposition behaviour of graded beds. Solid black curve shows the total bed shear stress due to wave breaking-induced turbulence, wave stirring and currents, as a function of water depth. Equilibrium critical stress curves (solid grey lines) are shown for bed layers of a single-size-fraction and two mixed grainsized fractions. Assuming no changes on deposition rate, the bed is eroded if total bed shear stress is larger than critical shear stress and bed is accreted if total bed shear stress is lower. This bed's responses are represented by grey arrows that show system trajectories towards stable (filled circles) or away from unstable points (empty circles).

4.2. Downward causation and emergent behaviour

The High Angle Wave Instability described above is also an example of how a local feedback can lead to both emergent landforms (capes) and emergent processes (wave shadowing). When a HAWI feedback loop dominates the local alongshore sediment transport overall feedback, it causes finite amplitude cuspate landforms to emerge from initial small perturbations. However, these features cause wave shadowing and influence the growth of adjacent features. This emergent process (wave shadowing) is unrelated to the initial instability and ends up controlling the alongshore sediment transport gradient at the smaller scale O(100 m). As noted by Coco and Murray (2007), this emergent non-local process implies that detailed analyses of the local surfzone processes that result in bulk alongshore transport will not lead to direct insights about how the large-scale shoreline features develop, nor will analyses confined to the analysis of the shoreline instability that causes features to grow initially. When the shoreline smoothing induced by small angle wave, HAWI and shadowing are included in a numerical modelling of initially straight shorelines under strongly asymmetric wave climate, cuspate spits develop and exhibit a striking array of non-local interactions (Ashton and Murray, 2006). Notably, these emergent spit features can dominate the alongshore sediment transport gradient behaviour for a considerable distance through shadowing effects.

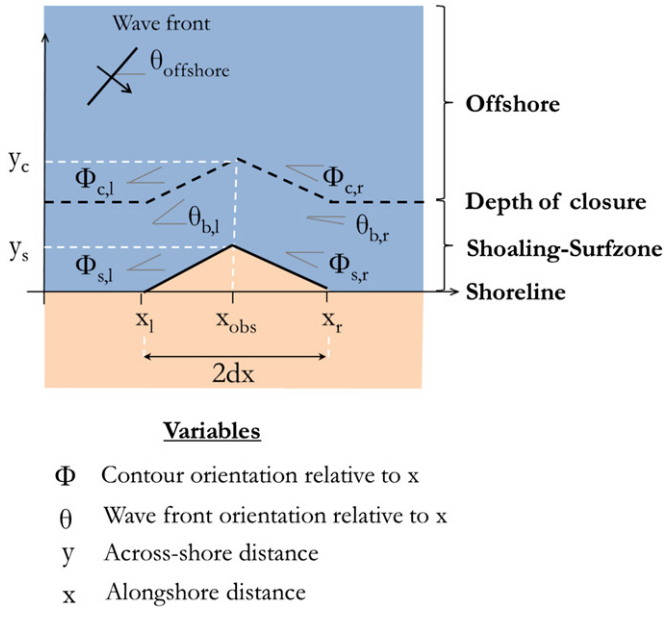

Fig. 9. Open coast plan-form schematization of a perturbation on the shoreline position, y_s, and depth of closure, y_c, at the observation long-shore location, x_{obs}. A central difference scheme is used to obtain the alongshore sediment transport gradient at the observation point for any given offshore wave angle. The sub-indexes b, c, s, correspond with variables at breaking, closure and shoreline respectively and the sub-indexes obs, l and r correspond with variables at the observation point and left and right of observation point.

The effect of wave shadowing (a non-local process) on the local feedback structure shown in Fig. 10d is acknowledged as an influence link between the alongshore sediment transport and itself. An unsigned link is used since wave shadowing can induce both an increase and a decrease of the local alongshore sediment transport gradient at different locations along the shoreline. This is best illustrated by reasoning how changes on the shoreline position at either the exposed shoreline, shoreline in the lee of the spit or shadowed shoreline might influence the alongshore sediment transport (Fig. 11). At both sides, the exposed side and in the lee of the spit, the schematization of shoreline shown on Fig. 9 is still valid, but since the local orientation might differ significantly from the global orientation, the definition of Q as positive along the global x-axis is no longer valid. In practice this is resolved by interpreting on which type of shoreline (exposed, in the lee of the spit

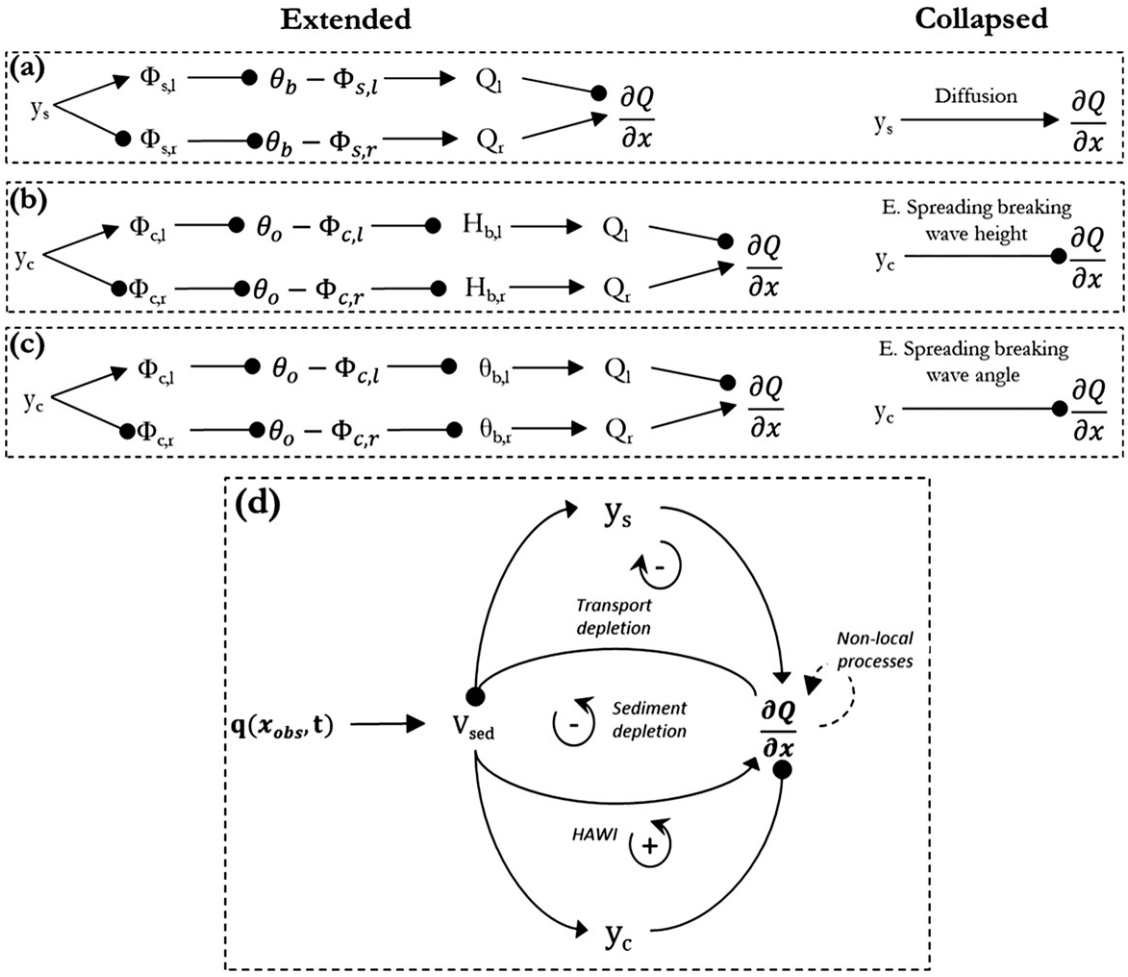

Fig. 10. Translation of the mathematical description given by Falqués et al. (2011) of the quasi 2D processes involved in shoreline High Angle Wave Instability into CLDs. A perturbation of the shoreline and the depth of closure line leads unambiguously to an increase (a) and decrease (b, c) of the alongshore sediment transport gradient respectively. (d) Shows the overall beach volume (V_{sed}) behaviour, where $q(x_c,t)$ represent a source/sink of sediment at the observation location.

or shadowed shoreline) the local shoreline is located (x_c) (e.g. Ashton and Murray, 2006). Since the directed graph shown in Fig. 10d is not spatially explicit, the type of local shoreline cannot be interpreted but is at least acknowledged as an influence link.

4.3. Linking model simplifications to model behavioural validity

An important application of CLDs is in revealing the limitations introduced by assumptions made in the formulation of a numerical process-based model. For example, let us assume that a modeller aims to reproduce the observed alongshore migration of a foreland such as the one shown in Fig. 12. Foreland dynamics are a product of a bidirectional wave climate and a simple segmented linear coastline (Burningham and French, 2014) so, in principle, both diffusive and anti-diffusive feedback loops might be active. A one-line model based on an assumed equilibrium profile is selected. To speed up the computation, the wave propagation algorithm is simplified by assuming the bathymetry is rectilinear and parallel to the shoreline. This ignores the wave shoaling that occurs between the wave breaking point and the depth of closure, which is needed to close the HAWI reinforcing feedback loop in the CLD. The resulting model will thus behave in purely diffusive way. The GENCADE model Hanson and Kraus (2011) will behave in this way. Only if the bathymetry is not simplified and use made of a numerical wave propagation model (Van den Berg et al., 2011), is the alongshore wave energy spreading that closes the feedback loop included (with the effect of significantly increasing the computation time). In contrast, the raster-based Coastal Evolution Model of Ashton and Murray (2006) explicitly encodes this behaviour in its otherwise more highly parameterized numerical scheme. CLDs are non-software specific and therefore cannot be used to assess if models with similar assumptions and simplifications but different parameterization will reproduce the same behaviour. However, analysis of the feedback factors (see above) provides a robust basis for comparative evaluation of alternative model formulations.

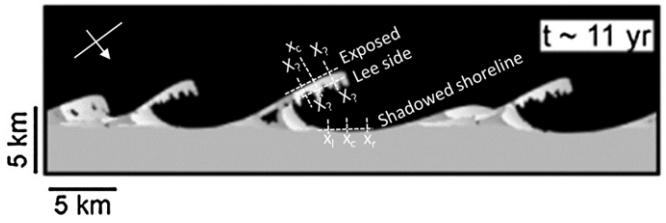

Fig. 11. Numerical result showing a snapshot plan view of an initially almost rectilinear beach after 11 years of strongly asymmetric wave forcing (more waves approaching from the left than the right). Arrow shows approximate direction of incoming waves approaching from the left.
Modified from Coco and Murray (2007).

Causal Loop Analysis is non-software specific and, in advance of the selection or formulation of a quantitative model, provides a means of identifying the important system behaviours that should emerge at the scales being simulated. While many features and some of the feedbacks depicted in a CLD appear self-evident, taken together the qualitative insights into aggregate system behaviour can prove illuminating and, as in the simple example presented above, these can be fundamental to the

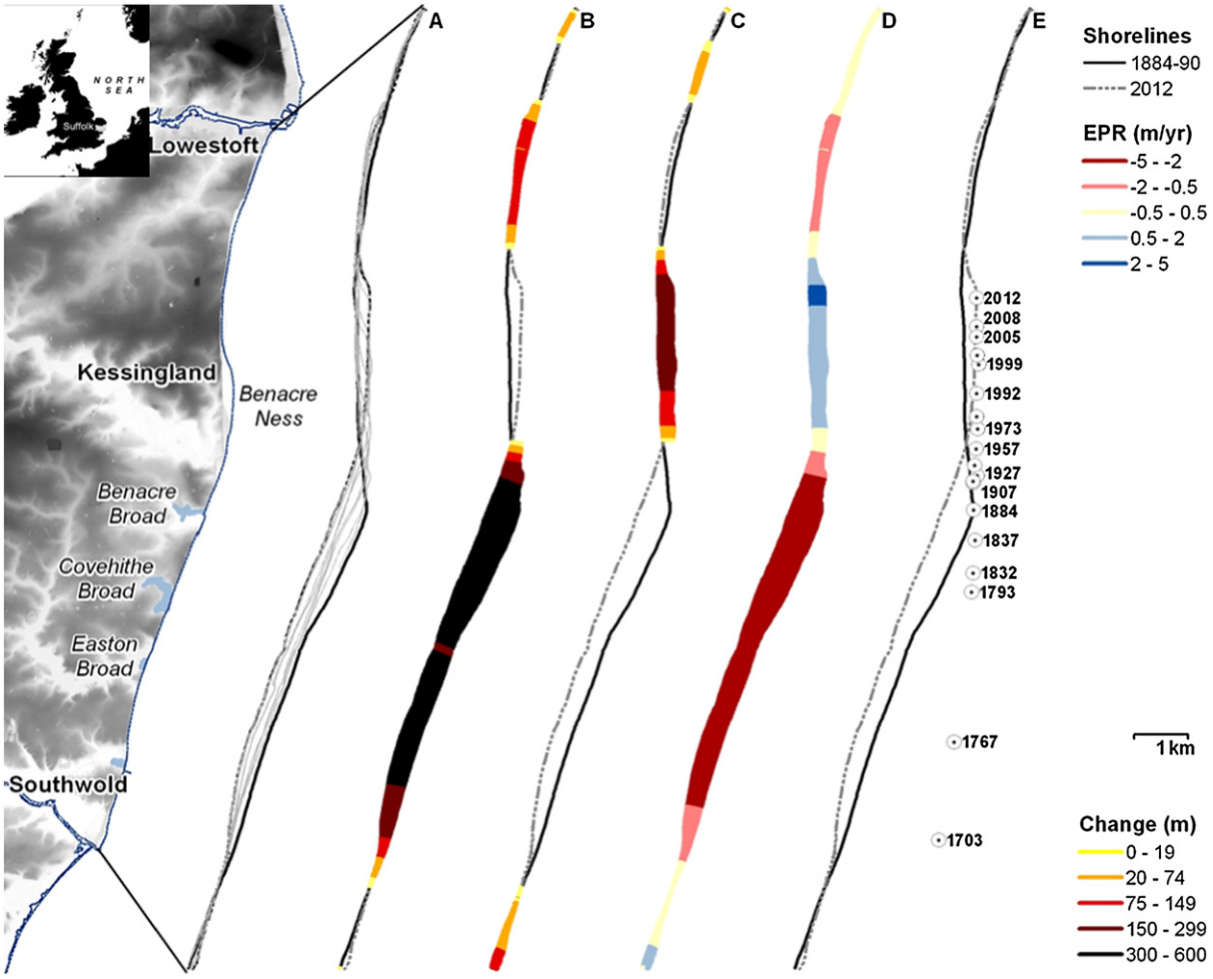

Fig. 12. Shoreline change analysis of the north Suffolk coast, showing historic migration of Benacre Ness foreland. A) Shoreline change envelope. B, C) net shoreline recession and advance. D) Historical end-point rate change. E) Historical change in the position of Benacre foreland.
Source: Burningham and French (2014).

explanation of the patterns of mesoscale coastal morphological change. Indeed, it can be argued that a lack of attention to anticipated system behaviours and a desire to obtain quantitative predictions irrespective of the robustness of the underlying model has led to weak and/or incomplete parameterizations that persist beyond their intended scope. The 'Bruun rule' is an obvious example that is noteworthy, not only for its continued application despite widespread criticism of its underlying assumptions (Cooper and Pilkey, 2004) but also for is embedded use in models that purport to offer more sophisticated insights into mesoscale coastal behaviour (French et al., 2016-in this issue).

5. Discussion and conclusions

The preceding analysis has highlighted the challenge, as well as the importance, of mapping some of the many feedbacks that govern coastal morphodynamics at decadal and longer timescales. Following Morecroft (1982), CLDs that represent systems as directed graphs are advocated as a means of distilling the cumulative effect of individual feedbacks that have been derived elsewhere by conceptualizing the parts of the system and simulating or observing their interaction. Essentially, this constitutes a knowledge formalisation process, in which a system-level understanding is synthesized from relevant scientific literature and observational data.

The case studies analysed herein are certainly not exhaustive but are intended to illustrate the advantages of applying a formal approach at two contrasting scales: (1) the erosion–accretion behaviour of graded (mixed) sediment beds, and (2) the local alongshore sediment fluxes of sand-rich shorelines. These case study examples are chosen on account of their central role in the quantitative modelling of geomorphological futures and as they illustrate different types of causation (upward causation, downward causation and emergent processes). To our knowledge, no similar qualitative behavioural modelling has been attempted for these geomorphological phenomena.

In this first example, we conceptualize the sediment bed elevation as a disequilibrium between erosion and accretion processes, and the local alongshore gradient as a disequilibrium between diffusive and anti-diffusive processes. This conceptualization aligns naturally with the pioneering work by Phillips (2009), whose framework recognises the possibility of multiple response pathways or trajectories, as well as multiple outcomes. In our case study of graded sediment beds, we show how up to three different outcomes (a null response, and two disequilibrium states) can be derived from a simple qualitative stability analysis. In the case of sand-rich shoreline planform behaviour, we show how two fundamentally different shoreline responses (diffusive and anti-diffusive) can be triggered by small changes of the shoreline cross-shore position. These responses have been described elsewhere using different numerical approaches (e.g. Ashton et al., 2001; Van den Berg et al., 2011).

The graded sediment study case also illustrates how a direct and non-direct upward causation can be mapped into a simple directed graph (Fig. 7). Upward causation, by which small-scale processes directly cause larger-scale, longer-term landscape evolution, has long been

used by geomorphologists to understand large-scale behaviour (Murray et al., 2014). As an example, the sedimentation–erosion balance of intertidal sediment has implications for the evolution of minerogenic-tidal flat morphology and the occurrence of a transition pathway to tidal saltmarsh (Friedrichs and Perry, 2001b; Fagherazzi et al., 2007). We have shown how a non-direct upward causation, the elevation deficit, can also be mapped as a directed graph. While not all feedbacks can be represented (either due to lack of understanding or for clarity seek), it can be acknowledged as an un-signed link as we have done for the feedback between ripple behaviour and bottom energy dissipation (e.g. Coco et al., 2007b).

The sand-rich local planform behaviour has been used to test how downward causation and emergent processes and landforms can be mapped as directed graphs. The growth of an initial small perturbation can be explained by the dominance of the HAWI feedback loop over the balancing feedbacks of the local alongshore sediment transport gradient. We have shown how the effect of wave shadowing, induced when the initial perturbation becomes large enough, is location-specific (exposed shoreline, lee of the spit, shadowed shoreline). Despite the directed graph not being spatially explicit, this downward causation can be represented as an un-signed link on the alongshore sediment transport itself. Spatially explicit numerical models overcome this issue by "interpreting the coastline" at each location (e.g. Ashton et al., 2001).

We believe that explicit depiction of feedback-structure diagrams is beneficial when exploring geomorphic futures with numerical models. System analysis and depiction of feedback structures is the first step of numerical modelling (e.g. Capobianco et al., 1999), but it is more often than not implicit and hence inaccessible. By explicitly mapping the feedbacks included and neglected within the model, the user is better positioned to assess whether or not relevant feedback loops are included. As an example, we have shown how model simplifications that appear intuitively independent (e.g. assuming bathymetry is rectilinear and parallel to the shoreline for speedy wave propagation of 1-line models) can limit modelled outcomes (e.g. a failure to resolve a critical HAWI loop in the case of shore planform evolution). The problem of how to assess the relative importance of a given feedback loop is the natural extension of the work presented here (e.g. Klocke et al., 2013; Payo et al., 2014).

Acknowledgements

We would like to acknowledge the useful discussions with Professor Brad Murray and Dr Laurent Amoudry during the preparation of this manuscript. This work was funded by the Natural Environment Research Council (NERC) as part of the Integrating COAstal Sediment SysTems (iCOASST) project (NE/J005541/1), with the Environment Agency as an embedded project stakeholder. The authors gratefully acknowledge helpful discussions with other iCOASST project team members and with the invited attendees of the iCOASST International Conference on Simulating Decadal Coastal Morphodynamics, held from 15 to 17 October 2013 in Southampton, UK.

References

Allen, J., 1999. Geological impacts on coastal wetland landscapes: some general effects of sediment autocompaction in the Holocene of northwest Europe. The Holocene 9 (1), 1–12.
Anfuso, G., 2005. Sediment- activation depth values for gentle and steep beaches. Mar. Geol. 220 (1), 101–112.
Ashton, A.D., Murray, A.B., 2006. High-angle wave instability and emergent shoreline shapes: 1. Modeling of sand waves, flying spits, and capes. J. Geophys. Res. Earth Surf. 111 (F4), F04011.
Ashton, A., Murray, A.B., Arnoult, O., 2001. Formation of coastline features by large-scale instabilities induced by high-angle waves. Nature 414 (6861), 296–300.
Benson, T., French, J.R., 2007. InSiPID: a new low-cost instrument for in situ particle size measurements in estuarine and coastal waters. J. Sea Res. 58 (3), 167–188.
Brain, M.J., Long, A.J., Petley, D.N., Horton, B.P., Allison, R.J., 2011. Compression behaviour of minerogenic low energy intertidal sediments. Sediment. Geol. 233 (1–4), 28–41.
Burningham, H., French, J.R., 2014. Travelling forelands: complexities in drift and migration patterns. J. Coast. Res. 102–108.
Cahoon, D.R., Reed, D.J., Day Jr., J.W., 1995. Estimating shallow subsidence in microtidal salt marshes of the southeastern United States: Kaye and Barghoorn revisited. Mar. Geol. 128 (1), 1–9.
Capobianco, M., DeVriend, H.J., Nicholls, R.J., Stive, M.J.E., 1999. Coastal area impact and vulnerability assessment: the point of view of a morphodynamic modeller. J. Coast. Res. 15 (3), 701–716.
Coco, G., Murray, A.B., 2007. Patterns in the sand: from forcing templates to self-organization. Geomorphology 91 (3–4), 271–290.
Coco, G., Murray, A.B., Green, M.O., 2007a. Sorted bed forms as self-organized patterns: 1. Model development. J. Geophys. Res. Earth Surf. 112 (F3).
Coco, G., Murray, A.B., Green, M.O., Thieler, E.R., Hume, T., 2007b. Sorted bed forms as self-organized patterns: 2. Complex forcing scenarios. J. Geophys. Res. Earth Surf. 112 (F3).
Cooper, J.A.G., Pilkey, O.H., 2004. Sea-level rise and shoreline retreat: time to abandon the Bruun Rule. Glob. Planet. Chang. 43 (3), 157–171.
Eisma, D., 1991. Particle size of suspended matter in estuaries. Geo-Mar. Lett. 11 (3), 147–153.
Fagherazzi, S., Palermo, C., Rulli, M., Carniello, L., Defina, A., 2007. Wind waves in shallow microtidal basins and the dynamic equilibrium of tidal flats. J. Geophys. Res. Earth Surf. 112 (F2).
Falqués, A., Calvete, D., Ribas, F., 2011. Shoreline instability due to very oblique wave incidence: some remarks on the physics. J. Coast. Res. 27 (2), 291–295.
French, J., 2006. Tidal marsh sedimentation and resilience to environmental change: exploratory modelling of tidal, sea-level and sediment supply forcing in predominantly allochthonous systems. Mar. Geol. 235 (1), 119–136.
French, J., Payo, A., Murray, A.B., Orford, J., Elliot, M., Cowell, P.J., 2016. Appropriate complexity for the prediction of coastal and estuarine geomorphic behaviour at decadal to centennial scales. Gemorphology(iCOASST Special Issue) 256, 3–16 (in this issue).
Friedrichs, C., 2011. 3.06 Tidal Flat Morphodynamics: a Synthesis.
Friedrichs, C.T., Perry, J.E., 2001a. Tidal salt marsh morphodynamics: a synthesis. J. Coast. Res. 7–37.
Friedrichs, C.T., Perry, J.E., 2001b. A review of tidal salt marsh morphodynamics. AGU Spring, Meeting Abstracts, 1.
Guza, R.T., Inman, D.L., 1975. Edge waves and beach cusps. J. Geophys. Res. 80 (21), 2997–3012.
Hanson, H., Kraus, N.C., 2011. Long-term evolution of a long-term evolution model. J. Coast. Res. 118–129.
Hanson, H., Militello, A., 2005. Representation of nonerodible (hard) bottom in two-dimensional morphology change models. ERDC, CHL CHETN-IV-63. US Army Corps of Engineers.
Harris, C.K., Wiberg, P.L., 1997. Approaches to quantifying long-term continental shelf sediment transport with an example from the Northern California STRESS mid-shelf site. Cont. Shelf Res. 17 (11), 1389–1418.
Houser, C., Barrett, G., 2010. Divergent behavior of the swash zone in response to different foreshore slopes and nearshore states. Mar. Geol. 271 (1), 106–118.
Klocke, D., Quaas, J., Stevens, B., 2013. Assessment of different metrics for physical climate feedbacks. Observational, Theoretical and Computational Research on the Climate System 41(5) pp. 1173–1185.
Kobayashi, N., Johnson, B.D., 2001. Sand suspension, storage, advection, and settling in surf and swash zones. J. Geophys. Res. Oceans 106 (C5), 9363–9376.
Kobayashi, N., Payo, A., Schmied, L., 2008. Cross-shore suspended sand and bed load transport on beaches. J. Geophys. Res. Oceans 113 (C7), C07001.
Komar, P.D., 1998. Beach Processes and Sedimentation, 1998. Prentice Hall, Upper Saddle River, NJ.
Lane, D.C., 2000. Diagramming conventions in system dynamics. J. Oper. Res. Soc. 51 (2), 241–245.
Lane, S.N., 2013. 21st century climate change: where has all the geomorphology gone? Earth Surf. Process. Landf. 38 (1), 106–110.
Le Hir, P., Cayocca, F., Waeles, B., 2011. Dynamics of sand and mud mixtures: a multiprocess-based modelling strategy. Cont. Shelf Res. 31 (10), S135–S149.
Manning, A.J., Spearman, J.R., Whitehouse, R.J.S., Pidduck, E.L., Baugh, J.V., Spencer, K.L., 2013. Flocculation dynamics of mud: sand mixed suspensions. Sediment Transport Processes and Their Modelling Applications.
Morecroft, J.D., 1982. A critical review of diagramming tools for conceptualizing feedback system models. Dynamica 8 (1), 20–29.
Murray, A.B., Coco, G., Goldstein, E.B., 2014. Cause and effect in geomorphic systems: complex systems perspectives. Geomorphology 214, 1–9.
Nielsen, P., 1992. Coastal Bottom Boundary Layers and Sediment Transport. 4. World scientific.
Paterson, D., 1997. Biological mediation of sediment erodibility: ecology and physical dynamics. Cohesive sedimentspp. 215–229.
Payo, A., Hall, J., Dickson, M., Walkden, M.A., 2014. Feedback structure of cliff and shore platform morphodynamics. J. Coast. Conserv. 1–13.
Phillips, J.D., 2006. Deterministic chaos and historical geomorphology: a review and look forward. Geomorphology 76 (1), 109–121.
Phillips, J.D., 2009. Changes, perturbations, and responses in geomorphic systems. Prog. Phys. Geogr. 33 (1), 17–30.
Phillips, J.D., 2012. Synchronization and scale in geomorphic systems. Geomorphology 137 (1), 150–158.
Schumm, S.A., 1991. To Interpret The Earth : Ten Ways to be Wrong. Cambridge University Press, Cambridge.
Schumm, S.A., Lichty, R.W., 1965. Time, space, and causality in geomorphology. Am. J. Sci. 263 (2), 110–119.
Slingerland, R., 1981. Qualitative stability analysis of geologic systems, with an example from river hydraulic geometry. Geology 9 (10), 491–493.

Svendsen, I.A., Putrevu, U., 1994. Nearshore mixing and dispersion. Proc. R. Soc. Lond. Ser. A Math. Phys. Sci. 445 (1925), 561–576.
Townend, I., 2003. Coast and estuary behaviour systems. Coastal Sedimentpp. 1–14.
Van den Berg, N., Falqués, A., Ribas, F., 2011. Long-term evolution of nourished beaches under high angle wave conditions. J. Mar. Syst. 88 (1), 102–112.
van Ledden, M., Van Kesteren, W., Winterwerp, J., 2004. A conceptual framework for the erosion behaviour of sand–mud mixtures. Cont. Shelf Res. 24 (1), 1–11.
van Rijn, L.C., 2007. Unified view of sediment transport by currents and waves. III: Graded beds. J. Hydraul. Eng. 133 (7), 761–775.
van Rijn, L.C., Walstra, D.-J.R., van Ormondt, M., 2007. Unified view of sediment transport by currents and waves. IV: Application of morphodynamic model. J. Hydraul. Eng. 133 (7), 776–793.
Van Wijnen, H., Bakker, J., 2001. Long-term surface elevation change in salt marshes: a prediction of marsh response to future sea-level rise. Estuar. Coast. Shelf Sci. 52 (3), 381–390.
Yamada, F., Tateyama, R., Tsujimoto, G., Suenaga, S., Long, B., Pilote, C., 2013. Dynamic monitoring of physical models beach morphodynamics and sediment transport using X-ray CT scanning technique. J. Coast. Res., SI 65, 1617–1622.